CHALMERS
UNIVERSITY OF TECHNOLOGY

Microscopy for pH mapping in nanofluidic devices

Victor Enevold

DEPARTMENT OF PHYSICS

CHALMERS UNIVERSITY OF TECHNOLOGY

Gothenburg, Sweden 2025

www.chalmers.se

MASTER'S THESIS 2025

Microscopy for pH mapping in nanofluidic devices

Victor Enevold

CHALMERS
UNIVERSITY OF TECHNOLOGY

Department of Physics
Chemical Physics Division
CHALMERS UNIVERSITY OF TECHNOLOGY
Gothenburg, Sweden 2025

© Victor Enevold, 2025.

Supervisor: Bohdan Yeroshenko, Department of Physics
Examiner: Cristoph Langhammer, Department of Physics

Master's Thesis 2025
Department of Physics
Chalmers University of Technology
SE-412 96 Gothenburg

Typeset in LaTeX
Printed by Chalmers Reproservice
Gothenburg, Sweden 2025

Microscopy for pH mapping in nanofluidic devices
Victor Enevold
Department of Physics
Chalmers University of Technology

Abstract

Nanotechnology, along with related fields such as nanofluidics, is an area of science with much potential. Research into material properties at the nano-scale is driving innovation across various fields, such as the development of new drugs in medicine, and improvements to solar cells in the development of sustainable energy. This thesis examines the possibility of creating and measuring pH gradients in nanofluidic channels, as a novel method to study nanoparticles subjected to different pH environments. The presented process relies on fluorescence microscopy and a pair of double Amici prisms. When observing fluorescent particles or dyes in the nanochannels, the fluorescence is angularly dispersed by the prisms. This enables measurements that capture spatial distribution of particles along the nanochannels, and corresponding spectral information dispersed perpendicularly. The experiments confirm that it is possible to generate a pH gradient in the nanochannels, as well as to move it by applying pressure to the ends on the channels. The presented results are largely based on the use of the pH-sensitive fluorescent dye SNARF-1, and a foundation for future study with nanoparticle FRET probes is also provided.

Keywords: Nanofluidics, Fluorescence, Microscopy, Amici prism, SNARF-1, pH gradient

Acknowledgements

I want to thank my supervisor, Bohdan Yeroshenko, for all of the help I've received throughout the project. Your small adjustments to the setup often put me back on track after I'd gotten lost at the microscope, and you've given me many insightful answers to questions I didn't even know to ask. Finally, I want to thank to my examiner Christoph Langhammer for the opportunity to work with this project.

Victor Enevold, Gothenburg, June 2025

List of Acronyms

Below is the list of acronyms that have been used throughout this thesis listed in alphabetical order:

DAP	Double Amici Prism
FRET	Förster Resonance Energy Transfer
NP	Nanoparticle
PBS	Phosphate-Buffered Saline
RPA	Relative Prism Angle
SNARF	Seminaphthorhodafluors

Contents

List of Figures

List of Tables

1

Introduction

1.1 Material properties at the nano scale

It is easy to assume that material properties are unchanging, regardless of the size of the material under observation. However, this is not the case at the nanoscale. Consider gold, a highly noble metal. Jewelry made of gold can last centuries while still looking like the day it was made, a property stemming from gold's chemical inertness. Yet, when the size of the golden object is shrunken down to the nanoscale its properties begin to change.
For instance, when gold nanoparticles on a surface approach the size of $10\,\mathrm{nm}$ or smaller, they stop being chemically inert and start to show catalytic properties. One example of this is described [1], where gold nanoparticles are used to catalyze the reaction of CO_2 into CO. This is one example of how new material properties can be discovered at the nanoscale.
Nanotechnology is a topic that is in demand in many different fields of research. In medicine, it is key in the development of new drugs and diagnostic tools such as nanosensors [2]. It also plays a significant role in the transition from fossil fuels to green energy, as seen in the improvement of solar cells and the development of better hydrogen sensors, making the use of hydrogen fueled cars safer [3], [4].

1.2 Scope & Aim

The aim of this project is to examine a new way of studying nanoparticles. Specifically, this thesis studies if a pH gradient can be created and subsequently measured in a nanofluidic channel. Fluorescent markers sensitive to pH are introduced into the nanochannels, and observed by fluorescence microscopy. A pair of prisms with the property of inducing angular dispersion to light is utilized to enable the acquisition of spectral information, and thereby the pH, of each point along the nanochannels.
If it proves possible to create pH gradients in nanofluidic channels, this could potentially be used as a new method for studying the properties of nanoparticles in a changing environment. The studied particles could potentially both be flushed through the channels

and incorporated into the channel-walls. This work is heavily dependent on experimental work, and includes preparing the chemical solutions, optimizing the experimental setup, conducting measurements and analyzing the gathered data.

1.3 Overview

With the goal of imaging fluorescent markers to determine local pH values in nanofluidic channels, the underlying theory is presented in Chapter 2. The imaging technique, fluorescence microscopy, is shortly introduced followed by a description of the pair of double Amici prisms which are a key component of the experimental setup. Two fluorescent markers, a dye and FRET probes, are then presented. Surface passivation is discussed in order to minimize the amount of particles binding to the nanofluidic chips used. Chapter 3 covers the experimental setup and the methods used in the project, calibrating the angular dispersion, testing passivation methods and imaging pH gradients. In Chapter 4, the results of the studied questions are analyzed and discussed. A calibration between the wavelength of light and its corresponding dispersion in the measurements is presented, as well as images taken of the passivation methods and the pH gradient from the dye. The report is concluded in Chapter 5, where the work is summarized and an outlook for future progression on the project is offered.

2

Theory

2.1 Fluorescence microscopy

In this project, a combination of fluorescence- and darkfield microscopy is used to image fluorescent particles in nanofluidic channels. Fluorescence microscopy involves illuminating the sample with light at specific excitation wavelengths that match the absorption spectrum of the fluorophores being studied. When excited, these fluorophores emit light at longer wavelengths, which is then detected and used to generate an image. This method is closely related to darkfield spectroscopy. Unlike fluorescence microscopy, darkfield imaging is not limited to specific excitation wavelengths, and a broader spectrum light is used to illuminate the sample. Both methods share the characteristic that only the parts of the sample that emits light are imaged, leaving a black background that enhances contrast.

2.2 Nanofluidic chips

The experiments conducted in this thesis rely on the use of nanofluidic chips. The chips are based on a silicon substrate, and plasma etching is used to fabricate the nanoscopic features on the chip. After being etched, a layer of silicon dioxide is grown over the surface of the chip. Lastly, a cover slip of borosilicate glass is bonded to the chip, sealing the nanochannels [5]. The design of nanofluidic chips varies largely based on what they will be used to study. Chips can contain channels of different length, sizes, shapes and numbers. The chips also contain larger microchannels, acting as a step between the inlets in the back of the chip and the nanochannels.
The nanofluidic chips used in this thesis are illustrated in Figure 2.1. The size of the chip is approximately $1 \cdot 1\mathrm{cm}$. The chips have four inlets, pairwise connected via a microchannel. The two microchannels are connected by a large number of nanochannels with different sizes. As seen in Figure 2.1, the microchannels are curved so that there are two different lengths of nanochannels. The nanochannels varied between three sizes, $50 \cdot 50, 100 \cdot 100$ and $200 \cdot 200\mathrm{nm}$.

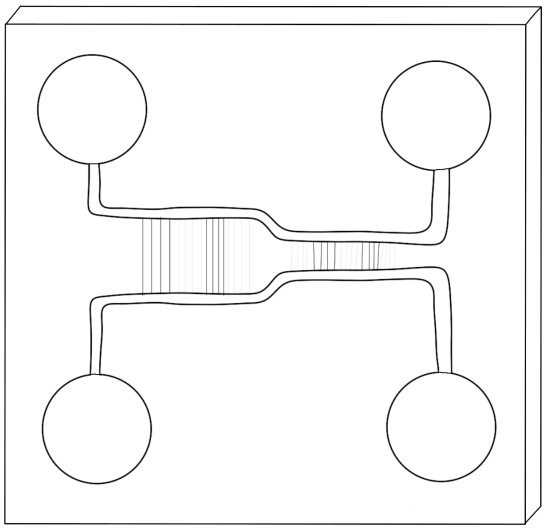

Figure 2.1: An illustration of the nanochips used in this project.

2.2.1 Piranha cleaning

Before use, chips can be cleaned with piranha to reduce any fluorescence from surface contaminants left from fabrication or storage. Piranha solution is a mixture of sulfuric acid, H_2SO_4, and hydrogen peroxide, H_2O_2, in a 3:1 ratio by volume. Piranha solution should be handled with utmost care due to its many risks. It is a strong oxidizing agent that aggressively dissolves organic matter, hence the name, likening its effect to that of the flesh consuming piranha. The process of preparing the solution is highly exothermic, easily reaching boiling temperatures and releasing corrosive fumes if the mixing is performed too quickly. Proper personal protection equipment such as a lab coat, gloves and safety goggles must be worn when handling piranha, and the use of piranha should be limited to within fume hoods [6].

2.3 Surface passivation

The layer of SiO_2 that the nanochannels are etched into is in many ways an optimal material. It forms a thin and even surface, and is both thermally and chemically stable. One way in which it is not a perfect material however, is that particles tend to adhere to the surface. The adhesion of particles, or adsorbates, to surfaces is caused by a number of different interactions. Adsorbates can bind chemically to surfaces, forming either ionic or covalent bonds. Other adhesion processes leave the chemical species of both adsorbate and surface intact, such as adhesion via Van der Waals forces or electrostatic attraction. Generally, adhesion of adsorbates to surfaces can occur on any surface, but the properties of the surface affect its adsorptive affinity. SiO_2 has some properties that favours adsorp-

tion. In the presence of water, SiO_2 undergoes hydroxylation, where water reacts with the SiO_2 surface to form sianol groups, $Si-OH$. These sianol groups make the surface hydrophilic and can deprotonate to impart a negative charge, increasing the adsorptive affinity for positively charged adsorbates. Additionally, the silanol groups serve as reactive sites for chemical binding.

In nanofluidics, adsorption is a problem. Particles can cause blockages, limiting the flow through the channels. The properties of particles that adhere to the surface can also change due to new molecular configurations and new forces acting upon them, creating a second unwanted signal. In order to limit the number of particles getting stuck, the surface can be passivated. Passivation is generally achieved by forming one or multiple layers that coat the surface and hinder other particles from adsorbing to the surface and the passivation layer itself. The passivation layers are generally formed by introducing chemicals that adhere to the surface, creating an inert interface between the surface and the fluids used in the channels. Two passivation methods are studied in this project.

The first method is using PLL-PEG. PLL-PEG is a co-polymer with a hydrophobic PLL-group and a hydrophilic and uncharged PEG group. The PLL group interacts electrostatically with the substrate, binding the co-polymer to the surface. The PEG group forms a densely packed polymeric brush that minimizes reactions between the liquid in the nanochannels and its surface [7]. A PEG brush is effective due to it forming a steric barrier, a non-reactive layer that physically shields the surface from adsorption.

The second method is an APS based passivation method [8]. In this method, the channel surface is introduced stepwise to three chemicals that build up a passivation layer. The first chemical is aminopropylsilatrane (APS), which creates a highly uniform layer of amines, forming covalent bonds with the surface. Secondly, SMCC, a click chemistry and cross-linker layer is used to prepare for the third layer which consists of PEG.

Due to its efficiency, both of the passivation methods use PEG as the interface between the fluid in the channel and the substrate. Should the passivation layers stay in place in the channels, the methods are expected to behave comparably. However, a difference between the methods is the way that the passivation layer is attached to the substrate. The strength of the electrostatically bound PLL-PEG, and the covalently bound APS are different, and not expected to behave identically when exposed to the acidic and basic environments that will be studied.

The level of success with the different passivation methods is tested by introducing a liquid containing avidin-fluorescein conjugate. This molecule consists of avidin, a biotin-binding protein that efficiently binds to surfaces, and fluorescein, which is a common fluorophore with a bright signal. For simplicity, avidin-fluorescein conjugate will be referred to as 'avidin' throughout this text.

2.4 Double Amici prisms & Angular dispersion

A key component of this project is the use of a pair of identical direct-vision prisms, also called double Amici prisms (DAPs). DAPs disperse light, which in this thesis is used to image the spectral information of fluorescent markers distributed along a nanofluidic channel.

A single Amici prism consists of two triangular prisms joined together. The materials of the prisms are chosen so that a central wavelength exits the prisms parallel to, but spatially translated from, the incident beam. Light of other wavelengths is dispersed along a line, but at other angles. If a single Amici prism is joined to a mirror image of itself, a DAP consisting of three triangular prisms is formed. Two main consequences of this are that the angular dispersion is increased, and that the center wavelength is refracted back to its original direction. The incident beam and the central wavelength emitted from the DAP therefore coincide on the optical axis.

When two DAPs are placed after each other, the total angular dispersion can be controlled by rotating them around the optical axis. If the two prisms are aligned so that the relative prism angle (RPA) is zero, the angular dispersion is twice that of a single DAP. When the RPA is $180°$, the DAPs counteract each other and the angular dispersion is canceled out. In this case the beam is returned back to its original state, apart from a fraction of light being absorbed by the prisms. By modulating the RPA between these two values the angular dispersion can be precisely controlled. This is illustrated in Figure 2.2. The direction of the dispersed light is dependent on the orientation of the DAPs, as seen in Figure 2.3. To keep the direction of the dispersion constant while changing the RPA, the DAPs must be counter-rotated by equal amounts.

This method of angularly dispersing light of different colors is useful in microscopy, as color can be used to convey different information. One example is when different fluorescent dyes are introduced to different cell types. This can be used to study cellular processes such as cell migration, endocytosis and phagocytosis. However, it is often necessary to filter out each color separately, building up a complete color image from many successive measurements. If the sample is unstable over time, this can introduce errors to the data. In certain cases, using DAPs to disperse light of different wavelengths can reduce the need for multiple measurements to a single picture. In this thesis, dispersing the emitted light from fluorescent particles enables the imaging of local spectral information used to measure local pH.

When working with DAPs, the value of the RPA is important. The angular dispersion must be large enough that two wavelengths of interest are separated enough to be individually identified. However, a larger angular dispersion also increases the signal-to-noise ratio.

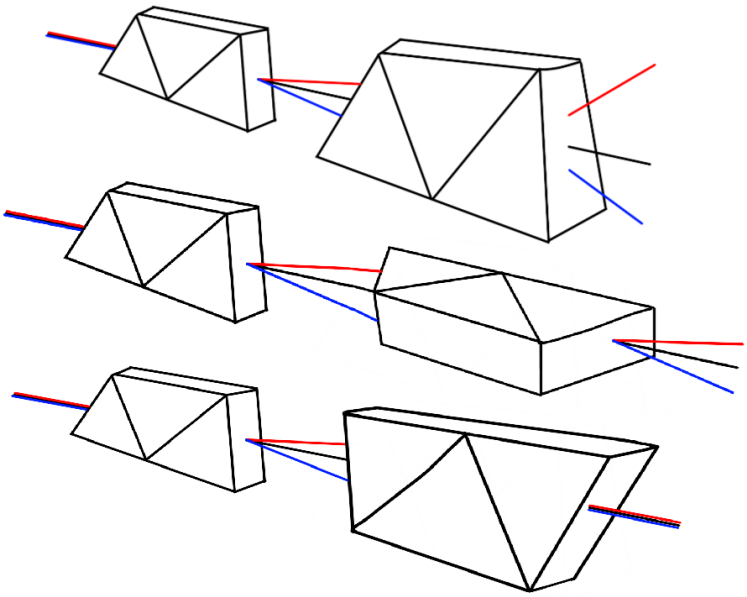

Figure 2.2: Three different configurations of a pair of DAPs. From top to bottom, the RPA is $0°$, $90°$ and $180°$. This affects the angular dispersion of the beam, going from strong dispersion to no dispersion. Note that the colors of the beam are chosen as a stylistic representation and do not reflect real optical behavior.

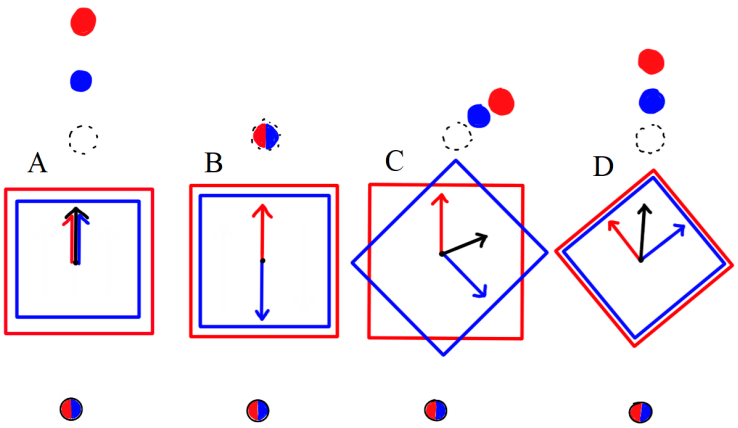

Figure 2.3: Four examples showing how the orientation of the DAPs affects the direction of the dispersed light. The DAPs are viewed and rotated around the optical axis. The red and blue arrows indicate the orientation of the DAP, and the black arrow shows the direction of dispersion. Note that the colors are chosen as a stylistic representation and do not reflect real optical behavior. The incoming beam is shown beneath the prisms, and the resulting dispersion appears above. The examples depict: maximum dispersion (A), no dispersion (B), large RPA dispersing on a diagonal (C) and counter rotated DAPs with a smaller RPA dispersing along the y-axis (D).

This is caused by having the same light intensity dispersed over a larger area on the sensor. Finding the optimal value of RPA must be made for each sample that is studied.
The use of DAPs is inspired by a method used in [9] where it is called "Continuously controlled spectral resolution". In this method the prisms are mounted on motorized rotators, allowing for the prisms to be rotated to exact RPAs without manually adjusting the components. This enables fine tuning, so that an optimal RPA for each measurement can be found, minimizing the signal-to-noise ratio.

2.5 Fluorescence

In order to measure the local pH values along the nanochannels, fluorescent markers are used. Fluorescence is a type of photoluminescence. On the atomic level, fluorescence occurs when light is absorbed by an atom, exciting an electron in the process. The electron is excited to one of several unstable excited states. Each electronic state is further divided into vibrational and rotational energy levels. After excitation, the relaxation process begins, taking the electron back to the ground state. One relaxation process is non-radiative vibrational relaxation, when vibrational energy is lost in as kinetic energy, taking the electron to a lower vibrational level. Another is internal conversion, a non-radiative relaxation that occurs when vibrational modes of different electronic levels overlap. After some energy has been lost, fluorescence occurs. This is the relaxation from a higher energy state back to the ground state via the emission of a photon. Due to the energy losses in the excited state, the emitted light has lower energy, and a longer wavelength than the absorbed light. The entire fluorescence process takes between 10^{-7} and 10^{-9} seconds.
In theory, fluorophores can fluoresce indefinitely. However, exposure to the exciting wavelengths increases the risk for photobleaching. Photobleaching is the irreversible destruction of fluorophores, resulting in the loss of fluorescence. Photobleaching is caused by changes in the chemical structure of the fluorophore. One common cause of photobleaching is photo-oxidation. Photo-oxidation occurs when the fluorophore is excited to an alternative triplet state, which is long lived, and more reactive than the usual singlet states involved in fluorescence. While in the triplet state, the fluorophore can react with oxygen, further suppressing emissions. Having the fluorophore exposed to oxygen also leads to oxygen toxicity, as reactions with oxygen generate reactive oxygen species. These are harmful for both any biological samples studied, as well as to fluorophores, causing degradation of fluorescent proteins.

2.5.1 Snarf-1

5-(and-6)-Carboxy SNARF™-1, hereinafter referred to as SNARF-1, is a fluorescent pH indicator developed by Molecular Probes. When subjected to environments of different pH levels, the dye's fluorescence undergoes a wavelength shift. This is due to the dye existing in two protonation states, a protonated and a deprotonated state. In acidic environments, the dye is in its protonated form, and in basic environments the dye molecules release a proton, changing the dye to its deprotonated state. The change in the molecular structure of the dye leads to a change in fluorescent properties, specifically a shift of the emitted wavelength. The ratio of protonated to deprotonated dye molecules determines the emission spectrum [10]. The emission spectrum of SNARF-1 is depicted in Figure 2.4. The dye has two prominent emission wavelengths, typically near $580\,\mathrm{nm}$ and $640\,\mathrm{nm}$. The dye can both be used in solution, its use case in this thesis, and loaded into cells. The dye's behavior has been documented in pH environments ranging from pH 6 and 9. Its behavior outside this pH-range is not documented.

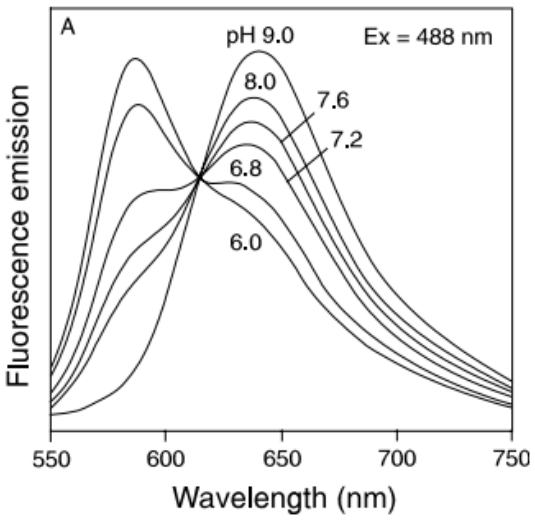

Figure 2.4: Emission spectrum of SNARF-1 excited at $488\,\mathrm{nm}$. SNARF-1 diluted to a concentration of $50\,\mathrm{mM}$ in potassium phosphate buffer at different pH values. Figure from SNARF-1 instruction manual [11].

2.5.2 FRET sensors

Förster Resonance Energy Transfer (FRET) is a phenomenon where energy is transferred non-radiatively between fluorophores. A donor fluorophore is excited by light, and by dipole-dipole coupling, the excitation energy is transferred to an acceptor fluorophore. This only works when the fluorophores are close, typically between 1 and $10\,\mathrm{nm}$ away from each other. FRET can be useful in multiple studies. Labeling different proteins

with donor and acceptor fluorophores can be used to measure protein interactions[12]. FRET can also be used to measure conformational changes as proteins undergoe different reactions [13]. The use of nanoparticle (NP) FRET probes in this thesis is mainly inspired by [14], where NPs loaded with thousands of donor dyes each are used to detect the presence of a target nucleic acid. On each NP, acceptor fluorophores are bound to the NP via twenty-three DNA oligonucleotides. In the absence of the target nucleic acid, the acceptors are within range to receive energy from the donors. When in contact with the target, the conformation of the DNA oligonucleotides changes, disabling FRET between the donors and acceptors. As the donor is a fluorophore, there is still a fluorescent signal, but consisting of other wavelengths. Due to the large ratio between the number of donors and acceptors, the signal from the acceptors is much brighter than in the cases with analogous FRET-based molecular probes, outperforming them by a factor of >2000 and another common detector, Qdots, by a factor of 100 [14].
NP FRET probes that respond to the pH of their environment, developed by the same group as in [14] at Strasbourg University, are used in this thesis. The probes made for [14] have been tested in the pH range of 4 and 8. Documentation about the pH sensitive probes has not yet been published, so the pH range is assumed to be comparable to those presented in [14]. Compared to the SNARF-1 dye, the NP probes are fewer in number, but with a brighter signal. The two fluorescent markers could therefore produce different results. The dye, containing a larger number of fluorophores might be seen as a method to measure the pH of larger parts of the channels, resulting in “continuous” results, while the few bright FRET probes might yield “discrete” results from very specific locations in the channels.

3

Methods

3.1 Experimental setup

The experimental setup consisted of a microscope constructed on an optical table (SmartTable® OTS™ UT2). The microscope platform RM21 (Mad City Labs) was used as a foundation for the optical setup. The microscope was compatible with two lasers as illumination sources simultaneously. The two lasers used were a $488\,\mathrm{nm}$ laser (Oxxius LBX 488 LaserBoxx) and a supercontinuum laser (NKT Photonics, SuperK EXTREME EXB-6). The supercontinuum laser was filtered through a tunable wavelength filter (NKT Photonics, SuperK VARIA). This filtered the light to a range from 400 to $840\,\mathrm{nm}$, with a minimum bandwidth of $10\,\mathrm{nm}$. The paths of the lasers were combined so that both could be used to image the sample simultaneously. A collection of lenses functions as a beam expander that can be enabled or disabled to illuminate a larger or smaller area of the sample. The incoming laser beam was redirected to the sample by a micromirror. A second micromirror filtered out refracted light. Scattered light and fluorescence were directed to one of two cameras by inserting a mirror to redirect the beam path. The sample was imaged either by a CMOS camera (Andor, Zyla) via a tube lens or with a qCMOS camera (HAMAMATSU ORCA-Quest qCMOS camera C15550).

If the laser was directed toward the Hamamatsu camera, the light passed through two DAPs in front of the camera. Both DAPs were installed on rotational mounts and could be rotated individually, thereby allowing the modulation of angular dispersion. This was the camera that was mainly used, and all measurements taken with dispersion were captured by it.

The nanofluidic chip was mounted in a chuck above the microscope objective. The chuck contains a Teflon reservoir block that aligns four reservoirs with the four inlets of the nanofluidic chip. O-rings ensure a liquid- and gas-tight seal between the chip and the Teflon block, and between the block and chuck. The chuck was connected to a Microfluidic Flow Control System (Fluigent MFCS-EX) which enabled the precise control of gas pressure to the four inlets on the chip.

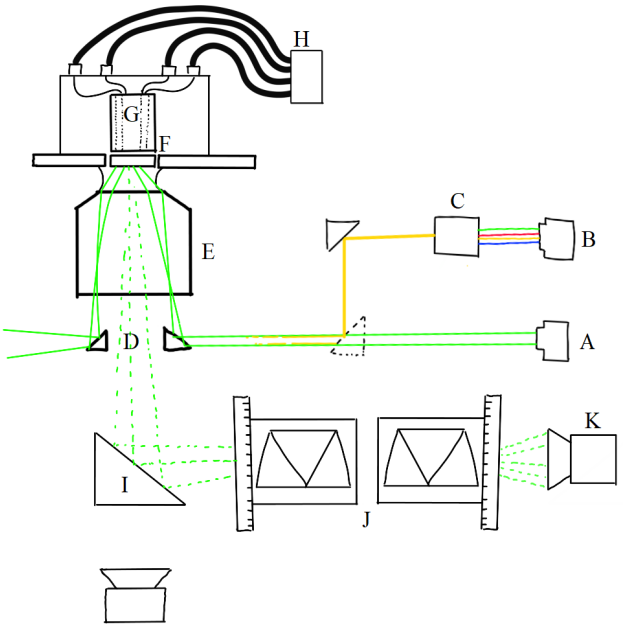

Figure 3.1: A schematic illustration of the experimental setup. The illumination sources, a 488nm laser (A) and the NKT laser (B) which is filtered by the VARIA(C), are combined and directed towards the micromirrors (D). A micromirror redirects the light through the objective lens (E) and to the nanofluidic chip (F). The Teflon block (G) holds any liquids that are to be introduced into the chip. A Microfluidic Flow Control System (H) is connected to the chuck via air-hoses. After the light has interacted with the chip, the unscattered light is redirected away by the other micromirror (D), and the light that has interacted with the chip hits the removable mirror (I). Following the mirror is a pair of DAPs on rotation mounts (J) and the qCMOS camera (K). Other components, such as the beam expander and a collection of filters that remove imperfections from the lasers are not depicted.

3.2 Passivation

Applying the passivation layers in both methods consists of flushing different chemicals through the chip for different amounts of time. For both methods, fresh chips were used. Initially, the nanofluidic chip was cleaned by submerging it in a piranha solution. Even though the chips were new and unused, the cleaning process has previously been shown to reduce autofluorescence, ensuring a better starting point for experiments. The piranha mixture was prepared in a fume hood by slowly adding hydrogen peroxide to sulfuric acid in a beaker until a 1:3 ratio by volume was reached. When the solution had cooled from its initial rise in temperature, the chips were placed in the beaker. The chips were left in the mixture overnight and were rinsed off before use the following day. When installed in the chuck, the channels were flushed with Milli-Q water to remove any remnants of the piranha-solution.

3.2.1 PLL-PEG

After the chip has been cleaned and the channels have been flushed out, the passivation process was started. The first mixture that was flushed into the channels was a $50\,\mathrm{mM}$ HEPES solution, diluted in Milli-Q water. HEPES is a buffering agent that prepares the surfaces for effective passivation. Thereafter, the PLL-PEG solution, consisting of $1\,\mathrm{mg/ml}$ PLL-PEG diluted in the HEPES solution, was flushed through the channels. Pressure was applied to two of the inlets, using $1500\,\mathrm{mbar}$ and $2500\,\mathrm{mbar}$, such that flow was established through both microchannels as well as the nanochannels due to the pressure difference in the surrounding microchannels. The PLL-PEG solution was flushed for 25 minutes before the direction of the flow was reversed and flushing continued for an additional 25 minutes. After this, the passivation layer should have formed, and the HEPES solution was flushed through the chip again to remove any unbound PLL-PEG.

3.2.2 APS-passivation

As with PLL-PEG passivation, the chip is first cleaned with piranha and flushed with Milli-Q water. The chip was then sequentially flushed with three solutions. The first solution was $115\,\mu\mathrm{M}$ APS diluted in ethanol. This was flushed through the channels for five minutes. The chip was then rinsed with ethanol before the second chemical, the cross-linking SMCC was used. The SMCC was diluted to a concentration of $1\,\mathrm{mg/ml}$ in a 10× dilution of PBS, phosphate-buffered saline, and flushed through the chip for 20 minutes. Once again, the chip was rinsed, this time with the 10× diluted PBS to remove unbound SMCC. Lastly, PEG diluted in a $0.9\,\mathrm{M}$ Na_2SO_4 solution to a concentration of $1\,\mathrm{mg/ml}$

was flushed through the chip. After the PEG solution had been flushed for an hour, the chip was rinsed with the 10× diluted PBS solution.

3.2.3 pH test

To test whether proper passivation of the channels had been achieved, avidin was diluted in PBS to a concentration of $50\ \mu\mathrm{g/ml}$ and flushed through the channels for 20 minutes. If the passivation was successful, little to no avidin should adhere to the channel walls. PBS was used to rinse out unbound avidin from the channels. The chip was then studied under the microscope. The NKT laser with wavelengths outside of avidin's absorption spectra was used to localize both the nanochannels and the microchannels. The $488\,\mathrm{nm}$ laser was then used to excite fluorescence in any avidin binding to the surfaces. The fluorescein label on avidin is very sensitive to bleaching, so exposing it to light for too long stops any fluorescence. A picture series of 50 images was taken, both in the microchannels and in the nanochannels. For these measurements, no dispersion was needed, and mirror I in Figure 3.1 was removed so that the Andor Zyla camera could be used instead of the Hamamatsu. As avidin is bleached during imaging, subtracting the last image from the first in series shows the fluorescence from avidin.
To test if the passivation withstands acidic environments, the channels were flushed with a HCl-solution diluted to pH 4 with Milli-Q water for 30 minutes. The acidity of pH 4 was chosen to match the NP FRET probes' lower pH-limit. After this, avidin and PBS were flushed through the channels before two series of images of the nanochannels and microchannels were taken as previously described.

3.3 Calibration of angular dispersion

To calibrate the angular dispersion a nanofluidic chip was mounted in the experimental setup, and the two lasers were activated. One of the lasers had a fixed wavelength of $488\,\mathrm{nm}$, while the NKT supercontinuum laser was set to have its minimum bandwidth of 10 nm, and used at wavelengths between 505 and $690\,\mathrm{nm}$. Firstly, the prisms were rotated to their non-dispersive mode. The microscope stage was moved so that the nanochannels could be seen, along with at least one "scatterer". A scatterer is either an impurity or an imperfection on the chip that scatters light. As these appear as dots, they were easier to handle than the long nanochannels stretching along the entire image. With the prisms in their non-dispersive mode, the images produced by the two lasers should align, causing the scatterers to be depicted on the same location.
Secondly, an RPA value of $176°$ was chosen to calibrate the angular dispersion. The microscope stage was moved so that three scatterers in one of the microchannels were

imaged. An image series where the wavelength of the NKT laser was increased from 505 to $690\,\mathrm{nm}$ in $5\,\mathrm{nm}$ increments was then taken. As the wavelength increased, each scatterer was split into two dots, as the scattered light of the different wavelengths was dispersed at different angles. The images were processed using MATLAB. First, the images were converted to binary black-and-white images with the function `graythresh` to isolate the scattered dots from the background. The function `regionprops` was used to find the central point of each dot. The distance between the centers of the dots belonging to the same scatterer was calculated, and the position of the dot scattered by the $488\,\mathrm{nm}$ laser was considered to be located at the zero-mark. A second-order polynomial equation was fitted to the datasets from all three scatterers. This calibration makes it possible to determine the wavelength of scattered light by its location relative to the location of light scattered by the $488\,\mathrm{nm}$ laser.

3.4 SNARF-1

One of the methods used to create and measure pH gradients in the chips was the use of SNARF-1. The SNARF-1 dye was delivered as a lyophilized solid, and was prepared by diluting it with Milli-Q water to a concentration of $1\,\mathrm{mg/ml}$. It was then split into multiple vials containing smaller amounts, and stored in the freezer wrapped in aluminum foil to shield against light. Before each day of experimenting, a new batch of dye was thawed, to ensure fresh, unbleached dye. The dye was diluted into liquids with different pH values. For the acidic solutions, hydrochloric acid, HCl, was diluted to the chosen pH level, and for the basic solutions, sodium hydroxide, NaOH, was diluted. A pH meter (Thermo Scientific™ Orion Lab Star PH111) was used to measure the pH of the solutions. The SNARF-1 was then added to the prepared pH solutions.

The measuring process began by installing a chip in the microscope and loading the reservoirs with dye solutions. The solutions were split so that the two inlets connected to each microchannel was loaded with one of the dye-solutions. Once the nanochannels had been located and the focus had been set in the microscope, pressure could be individually applied to each inlet. This pressure could be varied up to $4000\,\mathrm{mbar}$. The pressure was then varied between the different inlets, and pictures were taken whenever interesting features were seen. The use of DAPs led the fluorescence of the dye to be dispersed perpendicular to the nanochannels, and different RPA values were tested in the measurement process.

4

Results & Discussion

4.1 Reusing nanofluidic chips

For a large portion of the runtime of this project, the equipment used to produced the nanofluidic was damaged and out of service. This quickly led to a shortage of nanofluidic chips, and previously used chips had to be cleaned and reused whenever possible. Unused nanofluidic chips can be assumed to share the same properties and serve as a baseline to compare subsequent measurements with. During the measurements, it was observed that the cleanliness of the chips could not be reliably restored to the same level of new chips, or even consistently between cleaning cycles. This caused many of the measurements to be inconclusive and difficult to interpret, due to the lack of a stable baseline to compare against. To clean the chips, two solutions were used, piranha solution and Hellmanex® III.

4.1.1 Cleaning with Piranha

Until the failure of the chip fabrication, the cleaning procedure had been to submerge the chips in a piranha solution overnight before use. The piranha solution is supposed to remove organic material and other impurities in the channels. This method relies on capillary action to wet the entirety of the channels within the chip. A disadvantage of this is that gas is produced when piranha reacts with organic matter. Small bubbles of gas could therefore form a blockage in the channels, preventing the rest of the chip from being cleaned.

To solve this problem, a chuck designed to hold the chips while actively flushing the channels with piranha was ordered. To minimize the risk that is associated with the handling of the strong oxidizing agent that is piranha, the chuck was designed to use negative pressure. The chuck had two inlets that piranha was added to, and two outlets that was connected to a syringe. By using a syringe to apply negative pressure to the outlet, the piranha should be sucked through the chip. Each attempt to clean the chips in this chuck was limited to between five and ten minutes. The method of using a syringe was sub-

optimal, as small leaks in the system led to the syringe losing the pressure. Due to this, during each cleaning attempt, the syringe needed to be disconnected and reattached multiple times. The result of washing a chip that had been exposed to an avidin solution is seen in Figure 4.1. As can be seen in Figure 4.1b, the piranha did seem to have an effect on the remains in the channel. However, as this cleaning method required constant supervision it was deemed too time- and labor intensive to be effective. If the method was improved to the point where it could be started and left for a longer period of time, spanning hours instead of minutes, this might have proved to be more useful. A solution could be the use of a pump to continuously maintain a negative pressure, but the risk of introducing piranha into such a device could be dangerous.
Another note is that there was no way to guarantee that the chips are fully cleaned after using piranha. The presence of fluorescent particles in the chip can usually be seen by checking whether they fluoresces or not. However, as fluorescence measurements cannot distinguish between the absence of particles that has been removed by cleaning and particles that has been bleached, this is not a viable method to confirm if the chips are clean.

4.1.2 Cleaning with Hellmanex® III

Hellmanex® III, hereinafter referred to as Hellmanex, is an alkaline concentrate designed for cleaning cuvettes made of glass and quartz, as well as other optical parts [15]. After the conclusion that piranha cleaning was not sufficient to clean the chips fully, a solution of 2% Hellmanex was introduced to the chips. When this solution was flushed through the chip as it was observed in the microscope, particles could be seen flowing through microchannels that were previously suspected to be blocked. This led to the continued use of Hellmanex to further clean the channels. After rinsing a chip with Hellmanex, it was flushed with water to remove any leftovers of the cleaning agent.
While the use of Hellmanex initially seemed to be a good way of cleaning the chip, some suspicions began to rise regarding it towards the end of the project. Measurements that should have given clear results did not behave as expected. In Figure 4.2 the fluorescence from SNARF-1 solutions with both pH 6 and 11 are shown to emit light at the same wavelengths, but with different intensities. This behavior does not match the emission spectra for the SNARF-1 dye, as seen in Figure 2.4. This leads to the conclusion that something had caused the dye to stop functioning correctly. As the dye-solutions were prepared just before the measurements in the same way as before, the Hellmanex cleaning was isolated as a probable source. The chip was submerged in water until the following day where it was tested again, without being cleaned again first. This resulted in the successful measurements discussed in Section 4.4.3.

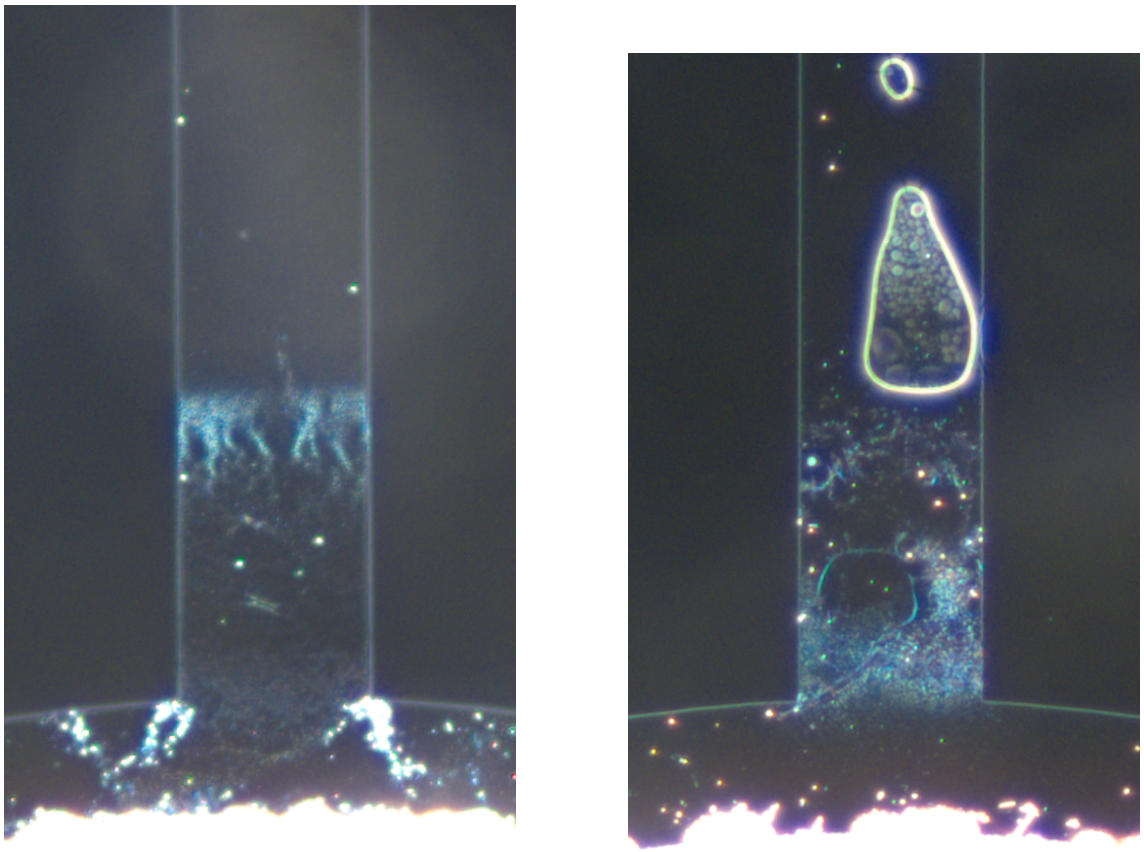

(a) This chip has had an avidin solution flushed through it, purposefully coating the channels. A structure resembling a total or partial blockage is seen in the microchannel.

(b) After the chip had been flushed with piranha three times for five minutes each the microchannel remained uncleaned. However, the dirty area is not identical to before the cleaning procedure.

Figure 4.1: Before and after images of cleaning a dirty chip with piranha. The bottom part of the images shows the bright inlet, with a microchannel extending from it. After the cleaning process, bubbles are visible, indicating that there has been a flow of piranha through the channels. The images were taken using a separate darkfield microscope.

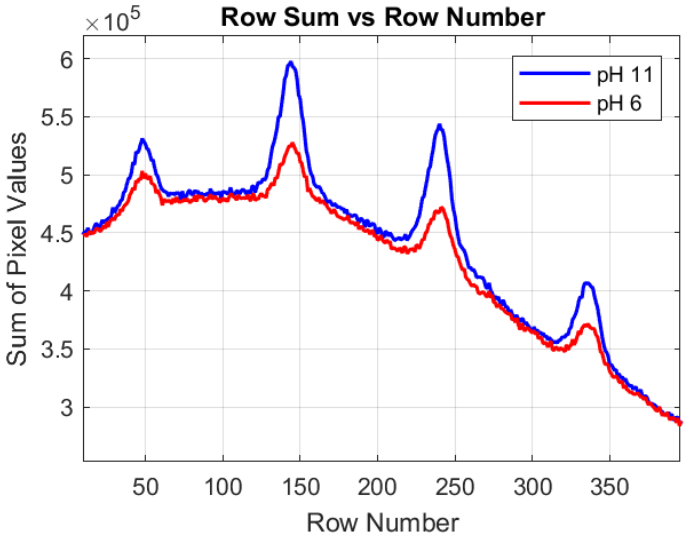

Figure 4.2: Summarized values for each row from fluorescence images of nanochannels. Each solution was flushed through the system for five minutes to rinse any remaining particles from within the channels before the measurement was taken.

4.2 Passivation

Both passivation methods were tested briefly. However, as discussed in Section 4.1, the supply of fresh nanofluidic chips needed for the measurements ran out due to equipment failure. This limitation ultimately resulted in the passivation methods not being used for fluorescence measurements.

4.2.1 PLL-PEG passivation.

The PLL-PEG passivation showed clear results both before and after the pH 4 solution had been flushed through the chip, both in the microchannels and nanochannels, depicted in Figure 4.3. Each histogram was made by subtracting the last image from the first in each image series, and summing the pixel values along each row. The two histograms in each figure represent different locations on the chip to avoid any influence from prior bleaching on subsequent measurements. Directly after the passivation, there is nearly no signal coming from either the nano- and microchannels, indicating that very little to no avidin bound to the surface. Passivation with PLL-PEG is therefore a possible method for neutral pH conditions. After the acidic solution had been flushed through the chips, the results deteriorated. There is fluorescence visible both in nano- and microchannels. Therefore, PLL-PEG passivation is unsuitable for use with solutions as acidic as pH 4.

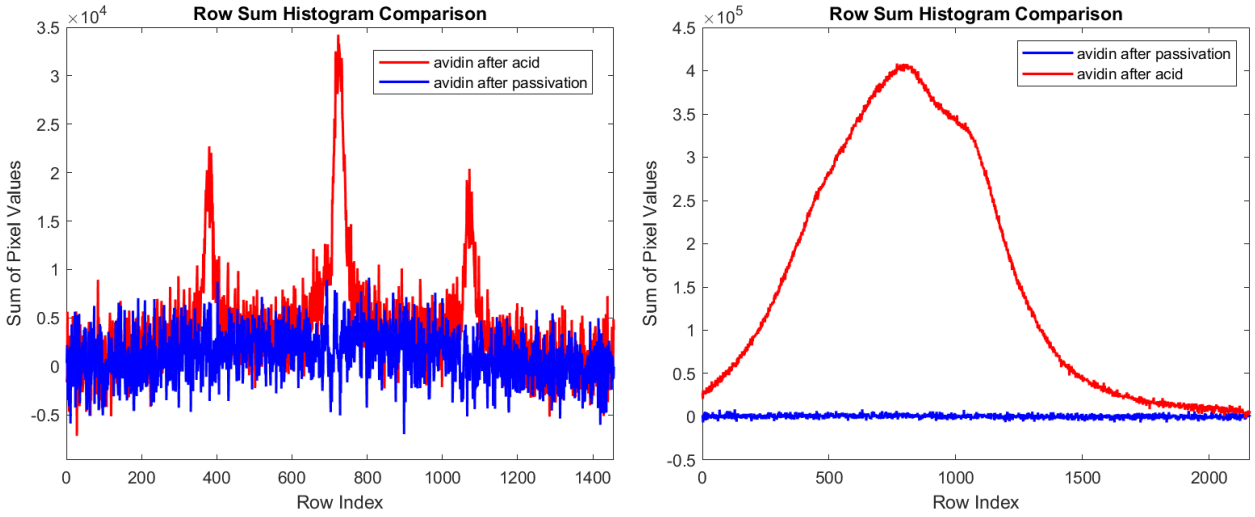

(a) A histogram depicting fluorescence from three nanochannels in the chip.

(b) Histogram in the microchannel region of the chip.

Figure 4.3: Histograms of avidin fluorescence signal intensity in a chip passivated with PLL-PEG.

4.2.2 APS-passivation

When the APS-passivation was tested, it did not match the expected results. When observing the microchannels after the avidin had been flushed through the chip, there was no stable baseline of the fluorescence. Instead, there seemed to be areas with three distinct levels of fluorescence intensity. In parts of the channels, there was no fluorescence at all, while other areas had two distinct levels of fluorescence. The edges of the areas were resembling bubble edges. One of the possible explanations was that there had been a problem with the piranha cleaning, as discussed in Chapter 4.1. After the chip had been submerged in piranha, it is possible that bubbles formed in the channels, and that the flushing of the passivation-chemicals was not enough to move them. The three levels could potentially be explained by a region in the chip having no gas bubble, a bubble on one of channel walls or a bubble covering the entire channel. The measurements, shown in Figure 4.4, show areas that were thought to have been passivated. The nanochannels display fluorescence both before and after the acid had been flushed through the channels. This suggests that the passivation was unsuccessful, however, the measurements from the microchannel show a clear difference between before and after the acid. The explanation that is deemed most likely is that bubbles had formed blockages in the imaged nanochannels, and that the passivation layer therefore did not form. In the microchannels, 4.4b, the peaks both before and after being flushed with acid come from scatterers that could be seen under the microscope. The high number of scatterers also indicates that the cleaning process had not fully worked. Apart from the scatterers, the rest of the measurement depicts a large difference in intensity between before and after the acid, indicating that the

APS-passivation also did not work in an environment with pH 4.

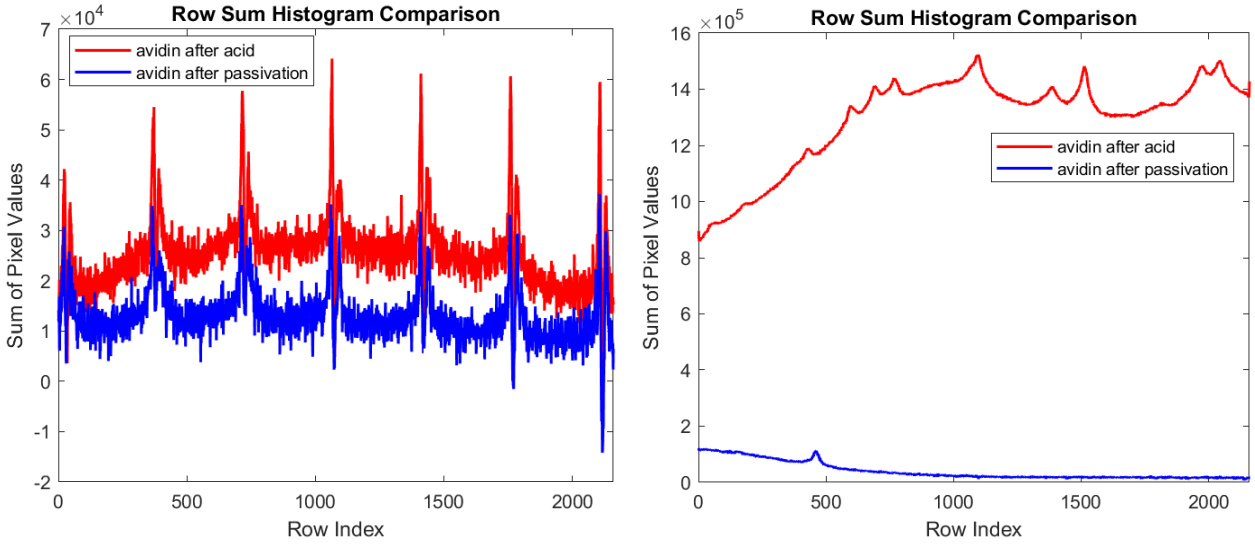

(a) Histogram in the nanochannel region of the chip.

(b) Histogram in the microchannel region of the chip.

Figure 4.4: Histograms of fluorescence signal intensity from avidin in chips passivated with the APS-based method.

Both passivation methods would be of interest to study further. The results did not conclude if one of the methods was better than the other, and a larger number of pH values would need to be tested to determine their usefulness. However, after the initial measurements, a combination of a lack of unused chips and the inability to clean previously used chips to a satisfactory level led to this part of the experiment coming to a close.

4.3 Angular dispersion from DAPs

When the prisms were in their non-dispersive mode, the two images from the different light sources were almost aligned. Rotating one of the prisms back and forth over small values of RPA showed that there was no position of the prisms that made the images align perfectly. This is probably due to small imperfections in the prisms and imperfect alignment of the two lasers. As the lasers are only used simultaneously to calibrate the dispersion and to locate features on the chip, a small deviation from alignment does not impact the final measurements.

One of the images in the image series with the 176° RPA configuration is seen in Figure 4.5. The light is dispersed along the vertical axis in the image, meaning that the dots on the same vertical line correspond to the same scatterer. The higher dot in each pair stays in place in all of the images, being scattered by the $488\,\mathrm{nm}$ laser. The lower dots come from scattering from the NKT laser. As the wavelength of the NKT laser increased, the

lower dots moved further down in the images, away from the $488\,\mathrm{nm}$ dot. Processing the dataset resulted in the graph presented in Figure 4.6. The calibration makes it possible to determine the wavelength of scattered light by its location relative to the location of light scattered by the $488\,\mathrm{nm}$ laser. An example of this is depicted in Figure 4.7, where both the nanochannels and a band of fluorescence can be seen. The distance between the scattered nanochannels and the upper limit of the band of fluorescence is approximately 40 pixels, indicating that the fluorescence ranges between approximately 488 and $570\,\mathrm{nm}$ as read from Figure 4.6. Note that Figure 4.7 was captured before the implementation of a new filter, which was later used to block light below $500\,\mathrm{nm}$, including the scattering from the nanochannels. When the locations of the scattered nanochannels were needed for comparisons, this filter was removed and an additional image was taken of only the nanochannels without moving the microscope to ensure that the imaged area stayed constant.

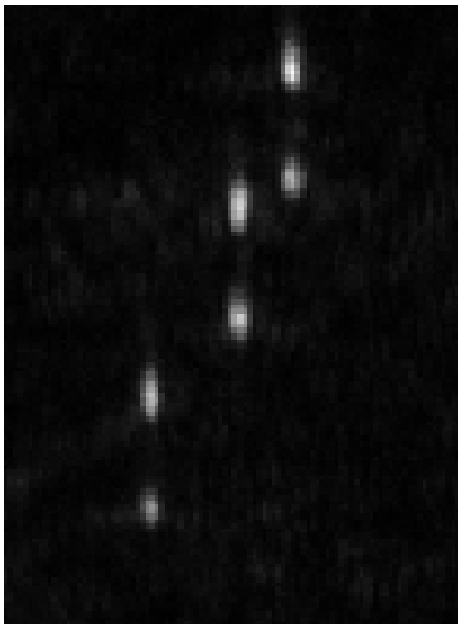

Figure 4.5: Three scatterers in the microchannel of a fluidic chip. Each scatterer is imaged in two positions due to scattered light of two wavelengths being angularly dispersed by the DAPs.

The rotation mounts holding the DAPs were graded in increments of $2°$. It was made clear early in the project that the most useful values of RPA were close to the non-dispersing $180°$ RPA setting, and that RPAs smaller than $170°$ caused the signal to get lost in the background noise. In order to be able to replicate the settings, the prisms were rotated only in $2°$ increments, significantly limiting the possibilities of finding an optimal RPA value. Furthermore, the propagation of error due to the lack of accuracy in rotating the DAPs to identical angles leads to a larger uncertainty in the RPA.

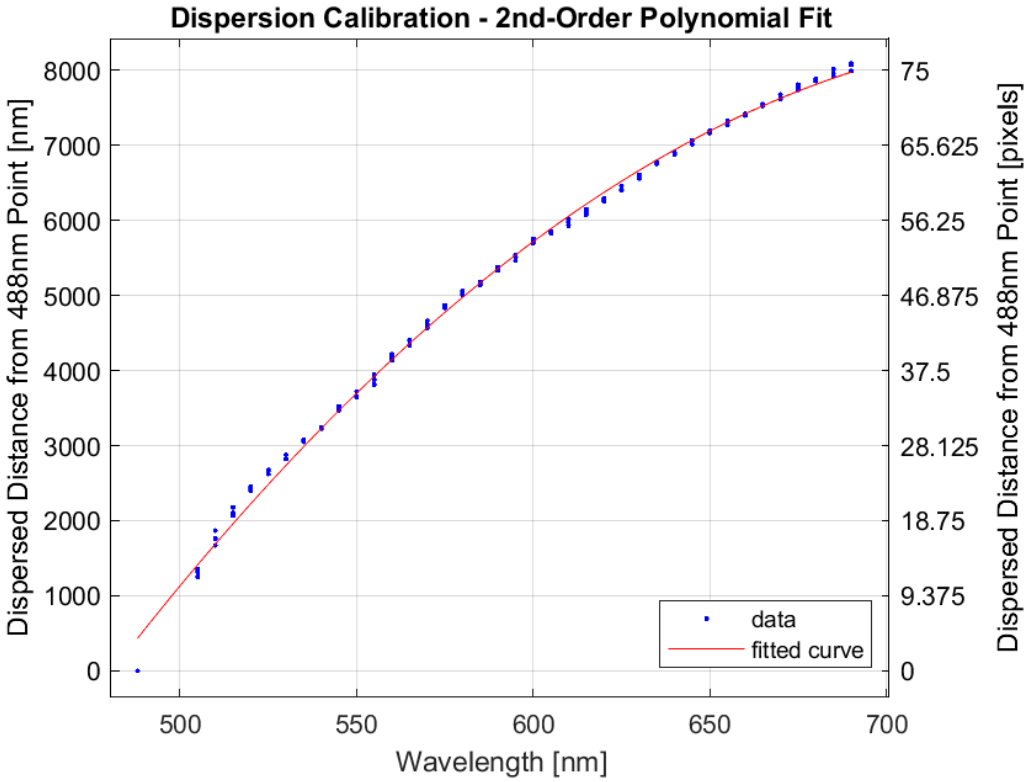

Figure 4.6: A second-order polynomial fit of the dispersion of different wavelengths on the sensor. The y-axes shows the distance between the scattered light of a given wavelength and the scattered light caused by the 488nm laser. This calibration corresponds to a RPA of $176°$

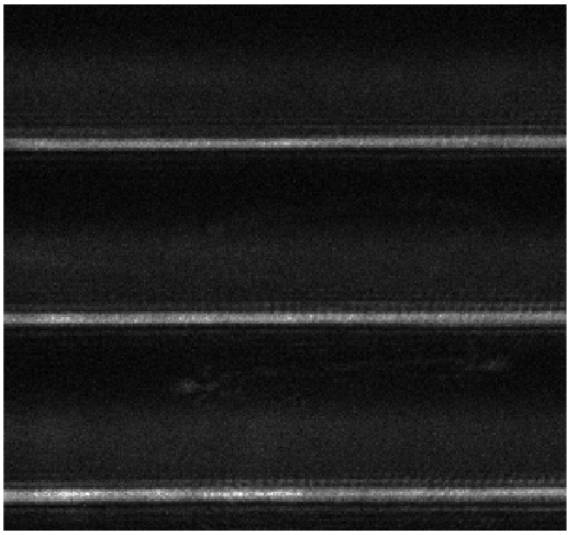

Figure 4.7: An image depicting three nanochannels and the fluorescent signal above each channel. The channels are imaged by scattered light. Nanochannels were flushed with a $0.01\,\mathrm{mg/ml}$ SNARF-1 in a pH 9 solution.

4.4 SNARF-1

The tests of SNARF-1 were also impacted by the lack of fresh chips, as discussed in Section 4.1. All of the results shown in this section come from measurements on the same chip, which was being cleaned with both piranha and Hellmanex up until Section 4.4.3.

4.4.1 pH solutions

The SNARF-1 dye was initially prepared in solutions at a concentration of $0.01\,\mathrm{mg/ml}$. This value was chosen as a starting point as the authors of [5] chose the concentration when using SNARF-1 in similar nanochannels. The dye was added to pH solutions that had already been prepared, with pH values of 6 and 9. When observed in the microscope, both solutions showed strong fluorescence. However, there was no apparent difference in their fluorescence. The samples were tested multiple times, and were flushed through the channels in different orders and durations. As seen in Figure 4.8a, the colors of the solutions were indistinguishable by the naked eye. As the dye has different molecular structures in its protonated and deprotonated form, one could expect a change in the color of the dye as well as a difference in its fluorescence when introduced to different pH environments. No documentation on the expected colour of the dye cold be found, but the identical colors of the solutions was considered suspicious.The combination of the identical measurements between the solutions and the similar colors led to the discovery that a fault had been made when preparing the solutions. It was assumed that the dye could be added to an already prepared pH solution without changing the pH. This proved not to be the case, which was verified by measuring the pH of the solutions. The measured pH values are seen in Table 4.1. As seen in the table, the solutions that were thought to have pH 6 and 9 were measured at pH 6.56 and 6.97 respectively. The relatively small difference in pH between the samples evidently did not cause a difference in color visible by the naked eye, and likewise the experimental setup might not be able to distinguish the fluorescence of liquids with such close pH values.

Two ways of addressing this were found. Either the solutions could be diluted further which should bring the pH closer to the intended values, or a solution more acidic or basic could be used as a starting point before mixing.

First, diluting the solutions was tested. As seen in Table 4.1, diluting the solutions further did not seem to bring the pH closer to the intended value. Comparing the pH of the two concentrations made with the “pH 6” solution shows that the pH value of the initial solution could not be six. This likely resulted from a lack of familiarity with the pH meter. When preparing the solutions that should have had pH 6 and 9, there was a difference

Table 4.1: The pH of the final dye-solutions were measured to differ from the assumed values. The solutions are continued to be referred to by their intended pH value, but the correct pH values are listed here.

Calculated pH without dye	Dye concentration [mg/ml]	Measured pH
6	0.01	6.56
6	0.001	7.02
9	0.01	6.97
11	0.01	10.46
11	0.001	10.32

between the readouts from the pH meter and standard pH paper. The pH meter was calibrated before each use, and should therefore provide a reliable result. There is a possibility that one of the calibrations failed, or that the equipment was used incorrectly. This uncertainty of the pH values complicates the comparison of the measurements from the nanochannels.

Diluting the solutions also resulted in weaker signals. In Figure 4.9, the original solutions were diluted by a factor of 100, to a dye concentration of $0.0001\,\mathrm{mg/ml}$. When the DAPs were configured in the non-dispersive state, a very weak fluorescence could be seen. The intensity of the signal was only slightly stronger than the background. When the DAPs were rotated into a dispersive mode, the fluorescent signal could not be seen against the background. A concentration of $0.001\,\mathrm{mg/ml}$ was also tested, and showed visible dispersion. However, as there was no indication that the weaker dilution was better than the original $0.01\,\mathrm{mg/ml}$ concentration, that was continued to be used.

An attempt was made using a more basic liquid as a starting point, with pH 11. A comparison between the colors of the pH 6 and pH 11 solutions is seen in Figure 4.8b. The noticeable difference in color indicated that this method had the potential to yield better results, however, no difference in fluorescence was observed using the new solutions.

4.4.2 Salt

After not seeing any wavelength shifts in the fluorescence of the different samples, for any combination of starting pH (6, 9, and 11) and dye concentration (10^{-2} and $10^{-3}\,\mathrm{mg/ml}$), a new parameter was tested. In [5], the pH shift in nanochannels depending on the ionic strength of the solutions is studied. The conclusion of the report is that solutions with low ionic strengths ($\approx 3\,\mathrm{mM}$), have a mean pH shift of approximately 1 pH unit. At higher ionic strengths ($\approx 150\,\mathrm{mM}$), the mean pH shift is reduced to just 0.1 pH units[5]. Since the tested pH solutions were assumed to have low ionic strength, this parameter was adjusted to investigate its potential effect on fluorescence. Samples containing $100\,\mathrm{mM}$ NaCl in addition to the dye were prepared and tested. However, there was no indication

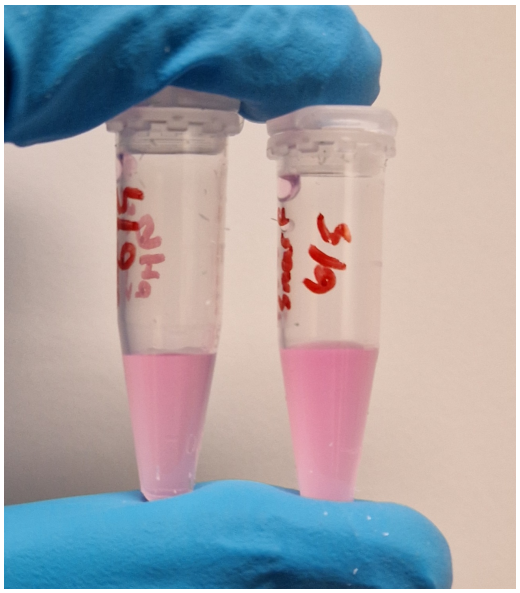

(a) A comparison between the dye-solutions with pH 6 (left) and pH 9 (right).

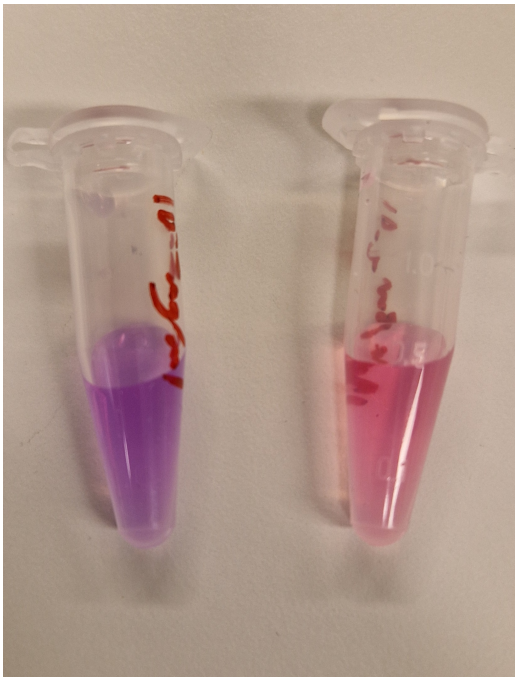

(b) A comparison between the dye-solutions with pH 11 (left) and pH 6 (right).

Figure 4.8: A comparison between the colors of the dye-solutions tested. The concentration of the dyes are $0.01\,\mathrm{mg/ml}$ in all vials.

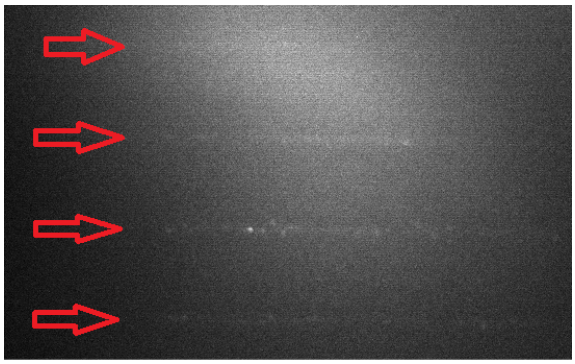

Figure 4.9: An image where a SNARF-1 dilution with the concentration $100\,\mu\mathrm{g/ml}$ is imaged with no dispersion, RPA $= 180$. The arrows indicate the location of four nanochannels, barely visible over the background.

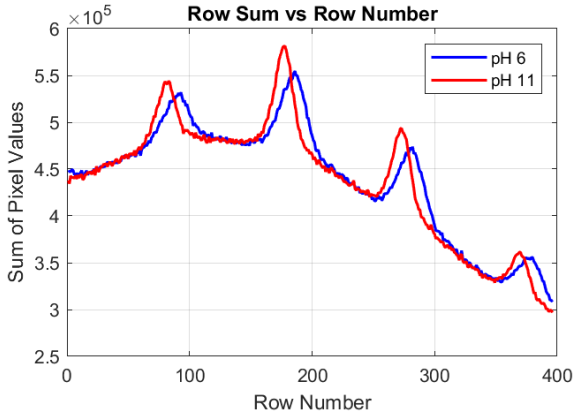

Figure 4.10: A visible shift in dispersed wavelengths, comparing fluorescence before and after a pH gradient was seen traveling through the nanochannels.

that this had any effect on the fluorescence. The pressure on the channels was varied so that the solutions were flushed from different directions, with different speeds and for different amounts of time. Nothing seemed to cause any difference in the fluorescence until the pressure on one of the inlets was increased and a pH gradient moved through the nanochannels in the image. The gradient had passed the channel before it could be captured in an image, but a picture was taken directly after the front had passed by, seen in Figure 4.10. This image was the first time the wavelengths of the fluorescence were seen to change. However, the shift could not be replicated by any method. Therefore, this is not a measurement that can be used to draw any firm conclusions. Later measurements that successfully showed a replicable pH gradient was achieved without adding any salt to the liquids. The test of including salt in the solutions neither confirms nor contradicts the results of [5], and would need to be tested more to be able to draw any conclusions.

4.4.3 pH gradient

After the chip had been washed with Hellmanex and tested with solutions containing salt, the chip was stored in water. The following day the test was repeated with the pH 6 and pH 11 solutions, with a dye concentration of 0.01 $\mathrm{mg/ml}$, and without any added NaCl. The chip was not cleaned before adding the solutions. This time, a distinct pH gradient moved through the nanochannels and the process was repeatable. Interestingly, the behavior varied depending on whether the pH 11 solution was flushed into channels that contained pH 6 solutions or vice versa. When the nanochannels contained pH 6 solution and the pH 11 solution was introduced, a distinct pH gradient was seen moving through the nanochannels, as depicted in Figure 4.11. In the opposite case, with pH 11 solution in the channels and introducing pH 6, there was no clear gradient moving through the channels. Instead, the fluorescence of the entire channel gradually seemed to shift simultaneously. When the pressure on the channels was turned off, and the liquids were left to diffuse through the channels, the distinct pH gradient reappeared in the center of the nanochannels.

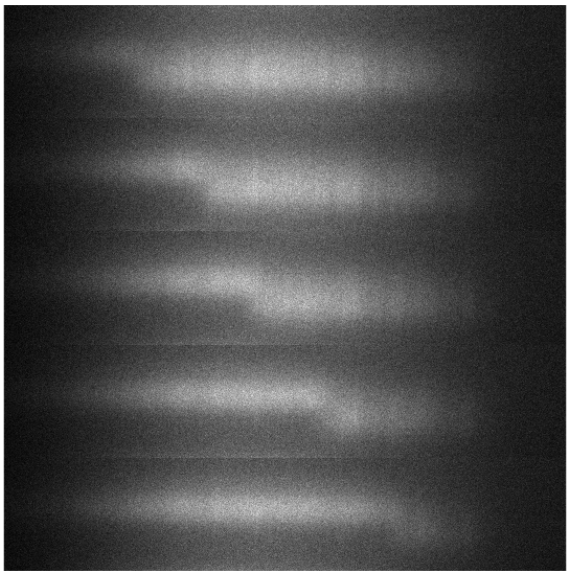

Figure 4.11: A nanochannel depicted in 5 points of time, with images stacked on top of each other. Each image was taken approximately one second after the previous one, showing (from top to bottom) the movement of the gradient through the channel. The channel originally contained a pH6-solution, and the gradient is moving from left to right as a pH 11 solution is pushed into the channel.

One of the images in the series of Figure 4.11 was analyzed, as seen in Figure 4.12. If the two peaks are assumed to be the $580\,\mathrm{nm}$ and $640\,\mathrm{nm}$ peaks depicted in Figure 2.4, the calibration in Figure 4.6 says that the peaks should be separated by approximately 19 pixels. In Figure 4.12b, the distance between the peaks is approximately 25 pixels. The

calibration and the measurements use different values of RPA. Since the RPA in Figure 4.12b is smaller, $172°$ compared to $176°$, it results in greater dispersion. Therefore, the conclusion that the peaks correspond to $580\,\mathrm{nm}$ and $640\,\mathrm{nm}$ can be considered plausible.

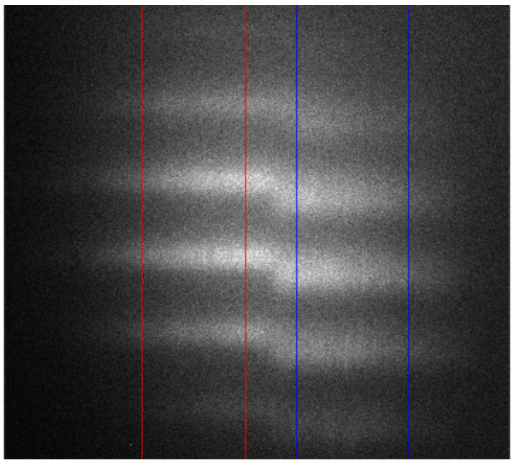

(a) An image with visible pH gradients in the center of multiple nanochannels

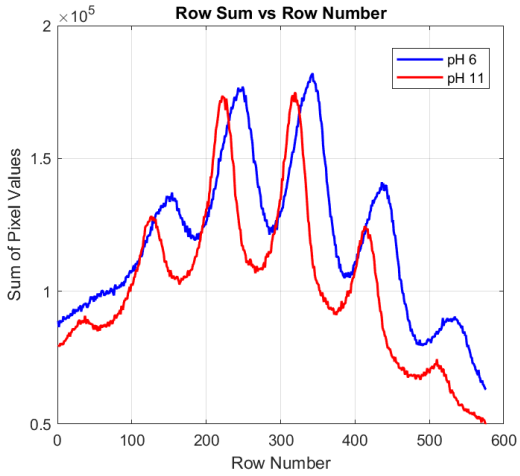

(b) Summation of the pixel values of each row within the markings of Figure 4.12a

Figure 4.12: A measurement showing fluorescent light from the SNARF-1 dye, dispersed onto the camera via the DAPs. RPA of $172°$

However, to measure the wavelength of the emitted fluorescence, the dispersed location must be compared to the position of $488\,\mathrm{nm}$ light. When the filter blocking light under $500\,\mathrm{nm}$ is removed, the scattered light from the nanochannels is imaged, as seen in Figure 4.13a. When the signal from the scattered nanochannels is overlaid onto Figure 4.12b, Figure 4.13b is produced. In this figure, the dispersed light from the nanochannels and the fluorescent light from the pH 11 solution appear in the same locations. This can be interpreted as though they consist of light of the same wavelength, which is not possible. The scattered light is known to be caused by the wavelength $488\,\mathrm{nm}$. As a filter blocking all light below $500\,\mathrm{nm}$ is used when imaging the fluorescence in Figure 4.12b, the pH 11-solution cannot produce visible fluorescence of this wavelength. Each fluorescent peak therefore has a higher wavelength, dispersed at a large enough angle to overlap with the nanochannel next to it. In Figure 4.13b, the peaks of both pH 6 and 11 solutions therefore correspond to the scattered nanochannel to their right. Interpreting the graph in this way, the peaks are ordered correctly when compared to the emission spectra in Figure 2.4. The emission of the more acidic solution has a shorter wavelength, dispersed closer to the scattered $488\,\mathrm{nm}$ line, than emission from more basic solutions. The dispersed distances are approximately 75 and 98 pixels for pH 6 and 11. This is larger than the dispersion seen in the calibration in Figure 4.6, but expected due to the difference in RPA-values. It is unfortunate that the dispersion from the pH-11 solution and the scattered nanochannels line up in Figure 4.13b as it decreases the clarity of the results. However, the RPA value can be increased to avoid replicating this overlap. This also highlights the potential benefit of conducting these measurements in nanofluidic chips with greater spacing between nanochannels, allowing the dispersed fluorescent light to fall between rather than on top of imaged nanochannels.

4.4.4 Dynamics of the change in fluorescence

The reaction speed of the fluorescence-shift was tested to see if the movement of the gradient could be explained. First, one of the solutions was flushed through the nanochannels until the entire channel fluoresced with the same pattern. The intensity of the laser was increased to $40\,\mathrm{mW}$ in order to bleach the fluorophores in the channel. The flow in the channels was then stopped by turning off the pressure. The fluorescence in the nanochannels slowly decreased in intensity as the dye was bleached. The pressure of the solution that had been flushed was then increased to $1000\,\mathrm{mbar}$. The intensity of the fluorescence in the channel immediately increased. From this, it could be concluded that there was a direct supply of new, unbleached fluorophores flowing through the entire channel immediately after the flow was turned on. This test was conducted with flow in the opposite direction through the channel as well, showing no directional dependence.

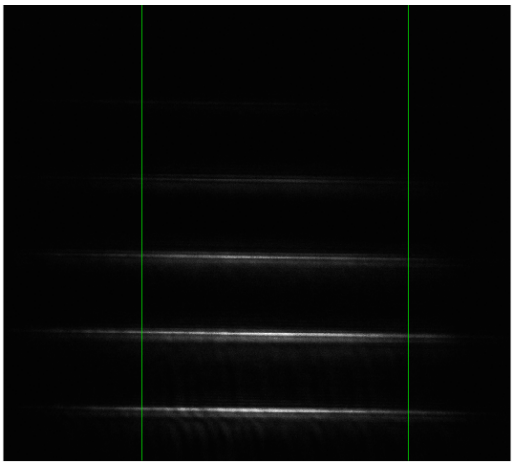

(a) Scattered light from nanochannels. Image taken at the same location as Figure 4.12a.

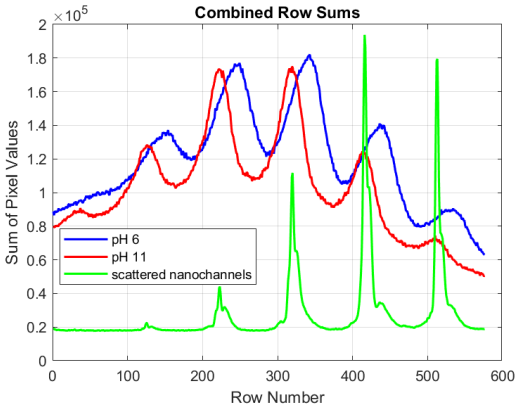

(b) Summation of the pixel values of each row within the markings of Figure 4.13a and 4.12b

Figure 4.13: A comparison between the results from Figure 4.12 and the scattered light from the nanochannels.

While the bleaching experiment showed that new fluorophores were introduced immediately, it did not confirm how the dye already in the channels reacted to flow. A dye solution was therefore flushed through the channel until the fluorescence stabilized. Water was then flushed through the channel. It took approximately 5 seconds of flushing with water for the fluorescence to completely disappear. This might indicate that the dye weakly adheres to the walls of the channel but is easily removed. If the fluorophores adhered to the channel walls with a stronger bond, the fluorescence would change in wavelength, adapting to the new pH of water. This shows that 'old' dye is flushed away relatively fast.

Then, the time for the pH gradient to move through the nanochannels was measured. When the nanochannels contained pH 6, and a solution with pH 11 was introduced by a pressure of $1000\,\mathrm{mbar}$, it took approximately 20 seconds for the pH gradient to move through the entire channel. When flushing pH 6 into channels containing pH 11, the time required was less clear, as no distinct gradient moved through the channels. However, after approximately 60 seconds, the fluorescence stabilized throughout the entire channel. A combination of the results of these three tests indicate that while the mass transport of liquid and fluorophores through the channels is fast, the transition between pH levels is delayed. It also shows that the change in pH depends on whether the shift is from acidic to basic conditions or vice versa. The different solutions were all water-based, rather than used with buffers that could potentially slow and stabilize pH changes in the channels. The silicon dioxide in the nanochannels has an intrinsic buffer capacity, discussed in [5], that could be affect the pH change. A more in-depth investigation of this behavior is

needed to draw any conclusions.

4.5 NP FRET probes

The amount of NP FRET probes that were designated to this project was limited. Measurements made before the start of this project indicated that the probes tended to adhere to the nanochannels, and that successful surface passivation would need to be established to use the probes as effectively. If no passivation could be achieved, the amount of probes was estimated to be sufficient for at most three or four measurements. Testing of the probes was therefore delayed while waiting for a successful cleaning method to be developed or for new chips to arrive. As the project drew to a close this had not occurred, and the focus was instead directed toward the measurement of SNARF-1.

4.6 Noise, Background and Signal strength

Throughout the experiment, the optical setup was calibrated multiple times and improved by the incorporation of filters that removed imperfections from the illumination sources. A filter blocking out light of wavelengths below $500\,\mathrm{nm}$ was installed after the first half of the project. This filter replaced an older variant that had a lower optical density. Before the filter change, scattering from the nanochannels was clearly visible, as seen in Figure 4.7. The new filter blocked this scattering, resulting in cleaner images, such as Figure 4.12a. Another consequence of the filter change was that a background signal coming from chip autofluorescence became distinguishable from the noise. The autofluorescence was not visible at low laser power, but became noticeable at $15\,\mathrm{mW}$ and above. The autofluorescence is depicted in Figure 4.14.
As described in Section 2.2, the studied nanofluidic chips contained nanochannels of various sizes. Although different channels were often compared, the measurements presented in this report are limited to those from the largest channels, as these provided the strongest signal.

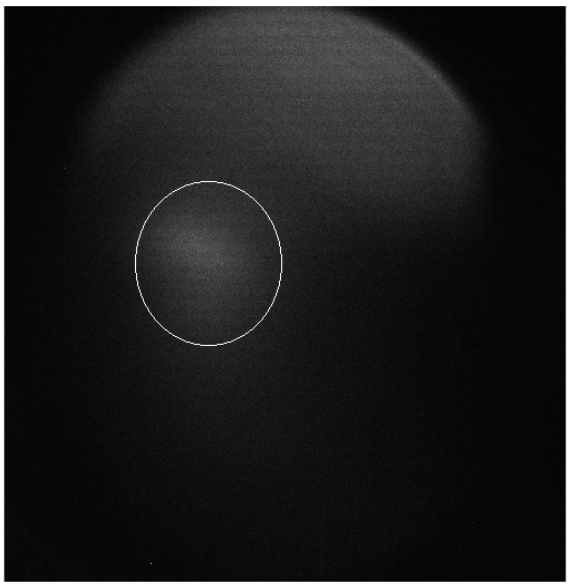

Figure 4.14: An image depicting what is believed to be autofluorescence from the borosilicate glass on the chip. The white oval indicates where in the frame the nanochannels are visible when imaged.

5

Conclusion

In this thesis, a method for measuring pH along channels in nanofluidic chips has been studied. Due to broken equipment, there was a shortage of the nanofluidic chips needed for the measurements. While this led to some of the experiments being cut short, such the investigation of surface passivation and NP FRET probes, test with SNARF-1 were successfully conducted, showing pH gradients in nanochannels.
Two surface passivation methods, PLL-PEG and APS-based passivation, have been tested. Both have been shown to work in neutral conditions but become nonfunctional after exposure to liquids with a pH value of 4.
A pair of Double Amici prisms has been used to disperse light, and a calibration between the location and wavelength of imaged light has been created for use in fluorescence microscopy. A second-order polynomial fit to the data makes it possible to predict the dispersed location of light in the range between 488 and $690\,\mathrm{nm}$. For fluorescent pH indicators, this enables the measurement of local pH values along nanofluidic channels.
Solutions containing the fluorescent dye SNARF-1 have been used to create visible pH gradients in the observed nanochannels. The gradients have been shown to spontaneously form in the zone between liquids of different pH values and to move when pressure is applied to either end of the channels. The movement of the pH gradient is also shown to be slower than the mass flow through the channels, and to be dependent on the direction of flow between basic and acidic solutions.

5.1 Outlook

Based on the results of this thesis it is clear that there is more to learn regarding pH gradients in nanochannels.
All of the measurements using old chips would benefit from being conducted again with new chips, ensuring a common reference point between the measurements.
The study would benefit from a further study of the emission spectra of SNARF-1 in order to conclusively identify the wavelengths corresponding to specific pH values. This could be used to validate the calibration between angular dispersion and wavelength. A

successful calibration can then be used to measure the pH of any point in the channel by using the ratios between the intensities of the two peaks in the emission spectra of SNARF-1.
It would be of interest to continue studying the kinetics of the pH gradient as the pH of the solution changes. The use of NP FRET sensors could also be explored to show how single particles in the channels react, compared to the SNARF-1 dye in which individual particles could not be distinguished.

Bibliography

[1] W. Zhu, R. Michalsky, Ö. Metin, *et al.*, "Monodisperse au nanoparticles for selective electrocatalytic reduction of co2 to co," *Journal of the American Chemical Society*, vol. 135, no. 45, pp. 16 833–16 836, 2013, PMID: 24156631. DOI: 10.1021/ja409445p. eprint: https://doi.org/10.1021/ja409445p. [Online]. Available: https://doi.org/10.1021/ja409445p.

[2] M. J. Mitchell, M. M. Billingsley, R. M. Haley, M. E. Wechsler, N. A. Peppas, and R. Langer, "Engineering precision nanoparticles for drug delivery," *Nature Reviews Drug Discovery*, vol. 20, no. 2, pp. 101–124, 2021, ISSN: 1474-1784. DOI: 10.1038/s41573-020-0090-8. [Online]. Available: https://doi.org/10.1038/s41573-020-0090-8.

[3] L. Wang, M. P. Teles, A. Arabkoohsar, *et al.*, "A holistic and state-of-the-art review of nanotechnology in solar cells," *Sustainable Energy Technologies and Assessments*, vol. 54, p. 102 864, 2022, ISSN: 2213-1388. DOI: https://doi.org/10.1016/j.seta.2022.102864. [Online]. Available: https://www.sciencedirect.com/science/article/pii/S2213138822009122.

[4] I. Darmadi, F. A. A. Nugroho, and C. Langhammer, "High-performance nanostructured palladium-based hydrogen sensors—current limitations and strategies for their mitigation," *ACS Sensors*, vol. 5, no. 11, pp. 3306–3327, 2020, ISSN: 2379-3694. DOI: 10.1021/acssensors.0c02019. [Online]. Available: https://doi.org/10.1021/acssensors.0c02019.

[5] D. Bottenus, Y.-J. Oh, S. M. Han, and C. F. Ivory, "Experimentally and theoretically observed native ph shifts in a nanochannel array," *Lab Chip*, vol. 9, pp. 219–231, 2 2009. DOI: 10.1039/B803278E. [Online]. Available: http://dx.doi.org/10.1039/B803278E.

[6] H. G. Schmidt, "Safe piranhas: A review of methods and protocols," *ACS Chemical Health & Safety*, vol. 29, no. 1, pp. 54–61, 2022. DOI: 10.1021/acs.chas.1c00094. eprint: https://doi.org/10.1021/acs.chas.1c00094. [Online]. Available: https://doi.org/10.1021/acs.chas.1c00094.

[7] SUSOS AG, *Pll-g-peg polymere - susos*, Accessed: 2025-03-11. [Online]. Available: https://susos.com/beschichtungstechnologien/pll-g-peg-polymere/.

[8] J. Andersson, J. Järlebark, S. KK, *et al.*, "Polymer brushes on silica nanostructures prepared by aminopropylsilatrane click chemistry: Superior antifouling and biofunctionality," *ACS Applied Materials & Interfaces*, vol. 15, no. 7, pp. 10 228–10 239, 2023, PMID: 36765467. DOI: 10.1021/acsami.2c21168. eprint: https://doi.org/10.1021/acsami.2c21168. [Online]. Available: https://doi.org/10.1021/acsami.2c21168.

[9] J. Jeffet, A. Ionescu, Y. Michaeli, *et al.*, "Multimodal single-molecule microscopy with continuously controlled spectral resolution," *Biophysical Reports*, vol. 1, no. 1, p. 100 013, 2021, ISSN: 2667-0747. DOI: https://doi.org/10.1016/j.bpr.2021.100013. [Online]. Available: https://www.sciencedirect.com/science/article/pii/S2667074721000136.

[10] C. S. Owen, "Comparison of spectrum-shifting intracellular ph probes 5'(and 6')-carboxy-10-dimethylamino-3-hydroxyspiro[7h-benzo[c]xanthene-7, 1'(3'h)-isobenzofuran]-3'-one and 2',7'-biscarboxyethyl-5(and 6)-carboxyfluorescein," *Analytical Biochemistry*, vol. 204, no. 1, pp. 65–71, 1992, ISSN: 0003-2697. DOI: 10.1016/0003-2697(92)90140-3. [Online]. Available: https://www.sciencedirect.com/science/article/pii/0003269792901403.

[11] Molecular Probes, Inc., *Snarf® ph indicators – product information*, Rev. Dec. 29, 2003. Available: https://www.thermofisher.com/order/catalog/product/C1270. Accessed: May 8, 2025, Thermo Fisher Scientific, Dec. 2003.

[12] A. Margineanu, J. J. Chan, D. J. Kelly, *et al.*, "Screening for protein-protein interactions using förster resonance energy transfer (fret) and fluorescence lifetime imaging microscopy (flim)," *Scientific Reports*, vol. 6, no. 1, p. 28 186, 2016, ISSN: 2045-2322. DOI: 10.1038/srep28186. [Online]. Available: https://doi.org/10.1038/srep28186.

[13] J. W. Gauer, S. LeBlanc, P. Hao, *et al.*, "Single-molecule fret to measure conformational dynamics of dna mismatch repair proteins," *Methods in Enzymology*, vol. 581, pp. 285–315, 2016, ISSN: 0076-6879. DOI: 10.1016/bs.mie.2016.08.012. [Online]. Available: https://doi.org/10.1016/bs.mie.2016.08.012.

[14] N. Melnychuk and A. S. Klymchenko, "Dna-functionalized dye-loaded polymeric nanoparticles: Ultrabright fret platform for amplified detection of nucleic acids," *Journal of the American Chemical Society*, vol. 140, no. 34, pp. 10 856–10 865, 2018, PMID: 30067022. DOI: 10.1021/jacs.8b05840. eprint: https:

//doi.org/10.1021/jacs.8b05840. [Online]. Available: https://doi.org/10.1021/jacs.8b05840.

[15] H. G. C. KG, *Hellmanex® iii special cleaning concentrate for cuvettes*, https://www.hellma.com/en/cuvettes-laboratory-supplies/laboratory-products/hellmanex-cleaning-concentrate, Accessed: May 23, 2025, 2025.

DEPARTMENT OF PHYSICS
CHALMERS UNIVERSITY OF TECHNOLOGY
Gothenburg, Sweden
www.chalmers.se

CHALMERS
UNIVERSITY OF TECHNOLOGY